International Journal of Engineering and Modern Technology (IJEMT) E-ISSN 2504-8848
P-ISSN 2695-2149 Vol 10. No. 11 2024 www.iiardjournals.org Online Version

Servo Valve Model Design Study for Aircraft Wing Flap Actuation Mechanism

Killabuko Peter A[1], Prof. Cuthbert Mhilu[2], Dr. Beltram Kiswaga[2], Geophrey Damson[3]
[1]Engineering Department, POLICE AIRWING, Dar es Salaam, Tanzania
[2]Department of Automotive and Mechanical Engineering, National Institute of Transport, Mabibo Street, P.O Box 705, Dar es Salaam, Tanzania
[3]Department of Research, TAFIRI, P.O Box 9750, Dar es Salaam, Tanzania
DOI:10.56201/ijemt.v10.no11.2024.pg159.184

Abstract

Take-offs and landings are critical phases of any flight since they require the best performance of all critical aircraft systems together with good cooperation and performance of the flight crew. Aircraft systems such as flight controls, communications, landing gear retraction, and extension, fuel systems must be effective at the phase of flight. Flight controls enable the flight crew to control the aircraft's direction and attitude. Secondary flight (Slats and flaps) controls help to argument lift. Aircraft flaps are attachments to the wing trailing edge designed to improve the aerodynamic efficiency of the wing at low speed. Flaps are extended at take-off to enable aircraft to take off at shorter distances. This study presents the design study of the servo valve model for the aircraft wing flap actuation mechanism, which plays a critical role in controlling lift and drag during flight operations. The main objective of this study is to design a servo valve model that accurately represents the dynamics of the servo valve for aircraft wing flap actuation mechanism. The study begins with an overview of the significance of wing flap actuation in modern aviation, emphasizing the need for precise control mechanisms to enhance aircraft performance and safety. A detailed literature review highlights common types of electrohydraulic servo valves existing, their design features, and their advantages and limitations. Also, various electrohydraulic motor and pump-operated system and their limitations established the motivation for a new approach. The mathematical model of the servo valve is derived using fundamental principles of fluid dynamics and control theory. It incorporates key parameters such as flow characteristics, pressure differentials, and response time. The model also addresses non-linear behaviors and feedback loops that arise in practical applications. By step inputs to each component of the servo valve, simulation studies have been conducted with the help of MATLAB computer program to observe their time response. By conducting simulation studies, the model facilitates the evaluation of servo valve performance. Simulation results demonstrate the effectiveness of the proposed model in predicting the valve's behavior under various operating conditions. The analysis shows how changes in input signals impact spool displacement and flow rate to the hydraulic motor for flap actuation, providing insights into the optimization of control strategies. Finally, the study discusses the implications of the model for future research and development, including potential applications in automated control systems and real-time monitoring. The findings underscore the importance of accurate mathematical modeling in enhancing the reliability and efficiency of aircraft control systems, ultimately contributing to advancements in aerospace engineering.

Keywords: *Servo Valve Model, Aircraft Wing, Flap Actuation, Aviation*

1.0 Introduction

Aircraft wings are parts of the aircraft with an aerofoil cross section capable of generating lift to enable the aircraft to fly. The wings generate lift when propelled in the air. Due to the presence of relative airflow against the wing, the amount of lift generated by the wing is proportional to the air density, the wing**'s** surface area, and the square of the airspeed. Wings are generally designed to be most efficient during a cruise, in most cases they are not well designed to be efficient for low airspeed flight (Meredith PT 1993). Low airspeed causes a reduction in the amount of lift generated by the wings, hence a reduction in the aircraft's ability to maintain safe flight. To compensate for the lift reduction at low airspeed flights such as the approach phase and maximizing the amount of lift generated by wings during take-off, wings are designed with high lift devices such as flaps and slats. A flap is a high-lift device used to reduce the stalling speed of an aircraft wing at a given weight (Smith AMO 1975).

Three types of flap kinematics are used to deflect the flaps as shown in Figure 1.1. Flaps can be deflected via a dropped hinge system in this case the flap's pivot is under the wing. If an aerodynamically optimum slot geometry is required for all flap positions, this cannot be achieved with a dropped hinge system, as a rule. A more complex version offers more possibilities: the flap is mounted on a carriage, which is moved on a track. A third type of flap design, essentially as a compromise between the two versions above, works with a linkage system.

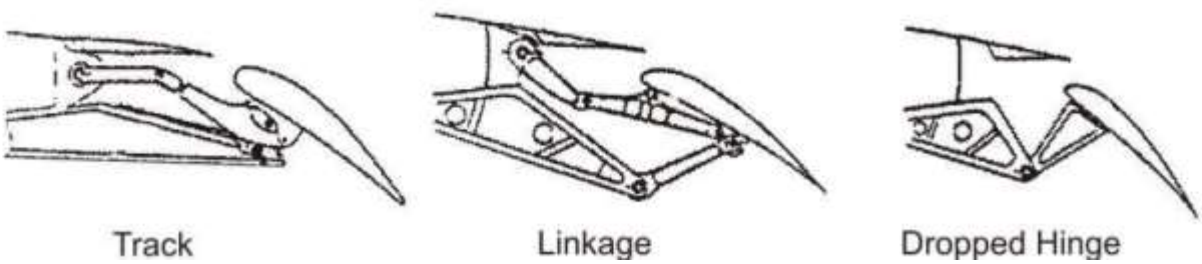

Figure 1.1: Flap kinematics of high lift systems (DATCOM 1978).

Flap mechanism in modern commercial aircraft consist of actuators mechanically connected via a transmission system across the wingspan, driven from a centralized power drive unit (J Hagen 2004). The flaps are connected to screw jacks which are operated by a primary drive shaft (Qiao et al 2018).

In Dash 8 Q400 aircraft, flap power unit actuated by flap selector, operates the flap drive system, and moves the flaps to their selected positions. The flap surfaces are electronically connected by the flap control unit and operated by number 1 hydraulic operated system. The flap control unit monitors and controls flap movement. The flap control unit is responsible for turning on the flap power and flap drive caution lights, it also turns on the standby hydraulic pump and the power transfer Unit when the flaps are moved outs of 0-degree position. The flap power unit converts hydraulic power to rotary mechanical power to operate the flap actuators, raising or lowering the flaps when selected (Q 400 Technical Manual 2018). The number 1 hydraulic system supplies pressure to the flap power unit. The `Flap Power Unit receives flap actuation signals from the flap control unit. It also sends feedback signals to let the FCU monitor flap movement. Consider Figure 1.3 below.

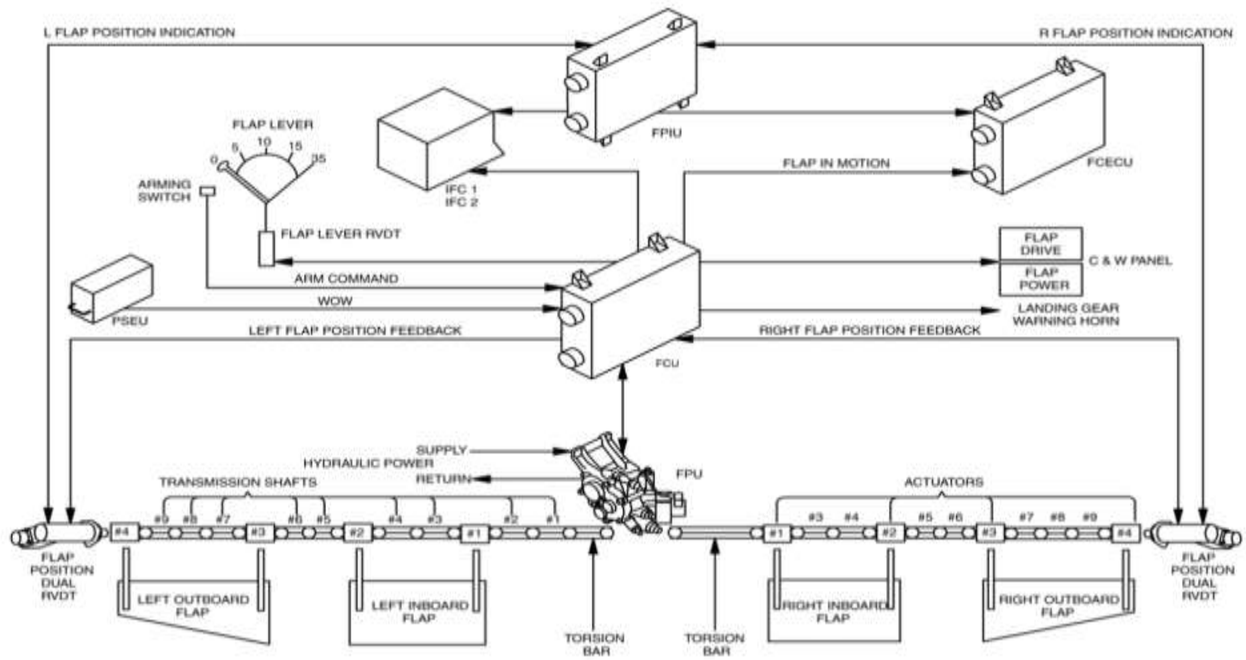

Figure 1.2: Dash 8 Q 400 Flap actuation Schematic Diagram (Q 400 Technical Manual 2018).

In Bombardier BD-500-1A10, the slat/flap electronic control units' control and monitor the high lift system. The slat/flap electronic control units receive slat and flap position inputs from the slat or flap control lever or the alternate flap switch and provide drive commands to position the slat and flaps accordingly. The slat/flap electronic control units determine the required system response and command for each channel of the PDU independently. The resulting drive from each PDU is summed at the differential gearbox to provide a single output to the transmission system. The feedback position sensor provides positional feedback of the transmission system to the slat/flap electronic control units. The PDUs provide the slat and flap actuation systems with mechanical power through an output shaft, as commanded by the slat/flap electronic control units, to drive the slat and flap surfaces against air loads and system friction. Strainers are located within the PDU to stop coarse debris from entering the control valves (BD-500-1A10 Technical Training Manual 2005).

Modern aircraft wing flap actuation mechanism links actuators with hydraulic or electric motor. A motor drives a linear actuator or rotary geared actuator. The rotary motion of the motor is coupled mechanically through a gearbox to an acrne lead screw, ball screw or planetary roller screw for conversion to linear motion. In a direct-drive versions, the motor is directly coupled to the screw mechanism without a gearbox.

The effective management of aircraft wing flaps is crucial for optimizing aerodynamic performance during various flight phases, including takeoff and landing. Wing flaps enhance lift and improve the aircraft's stability and control by altering the wing's shape and surface area. The actuation mechanism responsible for deploying and retracting these flaps must be both reliable and efficient, as it plays a pivotal role in ensuring the safety and performance of modern aircraft. The study focused on the design and modeling of a servo valve system tailored for the actuation mechanism of aircraft flaps. Servo valves serve as critical components in hydraulic systems, translating electrical signals into precise mechanical movements. By examining the dynamics of the flap actuation mechanism and the role of servo valves, this study aims to develop an optimized model that enhances responsiveness and accuracy in flap control.

Reducing the airspeed results in decreasing the amount of lift generated by the aircraft wings, hence reducing the aircraft's ability to maintain safe flight. With no flaps or mechanically failed flaps, the risk of stalling the aircraft during the final approach is greater. Optimum aerodynamic efficiency (lift-to-drag ratio) of an aircraft wing at low airspeed (approach speed) may be achieved by accurate control of the desired flap position during the approach and landing phase. Inaccurate positioning of the flaps may result in poor aerodynamic efficiency of the wing by producing an insufficient amount of lift for safe low-airspeed flight during the approach phase or an excessive amount of drag when deployed beyond the desired position leading to more fuel consumption. In a flap failure scenario (no flap approach), a large approach speed will be needed which may jeopardize the landing phase and may cause a hard landing which may damage the aircraft components such as the undercarriage unit, or may cause the aircraft to overshoot the runway during the ground roll after touch down. In this study, focus has been made on designing a Servo valve model for aircraft wing flap actuation mechanism for improving the aerodynamic efficiency of the wing during approach and landing phase of the flight.

Through comprehensive analysis and simulation, this research explored the interactions between the servo valve and the hydraulic system, addressing key performance metrics such as speed, reliability, and energy efficiency. The Servo valve model which has been designed in this study exhibits high dynamic performance suitable for application in aircraft wing flap actuation mechanism (extension and retraction of the flap) for accurate flap positioning and control. The outcome of this study is anticipated to contribute significantly to advancements in aircraft control systems, facilitating improved flight safety and operational efficiency in aviation.

2.0 Review of the paper

In the flap actuation mechanism of modern commercial aircraft, the control electronics instruct the operation of hydraulic control valves to set in motion hydraulic motors to move actuators via the transmission system. A Power Drive Unit (PDU) is used to convert hydraulic power into mechanical motion, often rotational, and drive an actuation system. Usually, a PDU is fitted with dual hydraulic motors each providing independent power to the transmission system via a speed-summing gearbox. Each motor is controlled by an independent motor supply via a dedicated valve block which ensures the hydraulic isolation between the two blocks (J Hagen 2004). The work herein describes the application of an Electrohydraulic Servo Valve (EHSV) within the valve block of the PDU of a flap system and presents a suitable EHSV type for use in aircraft wing flap actuation mechanism.

2.1 Electrohydraulic Servo Valve (EHSV).

Electrohydraulic servo valves, within the PDU valve blocks, provide directional control and control the acceleration and deceleration of the system. An enable valve is used to control hydraulic pressure to the torque motor controlled, electrohydraulic servo valve (EHSV). When the slat/flap electronic control unit energizes the enable valve solenoid, the enable spool valve opens, supplying hydraulic pressure. The slat/flap electronic control unit monitors the pressure supplied through a downstream pressure transducer. The hydraulic motor direction and speed are controlled by the EHSV, which is controlled by the slat/flap electronic control unit. Motor top speed is limited by a flow limiter valve in the return side of the EHSV. Consider Figure 2.1 below of a power drive unit.

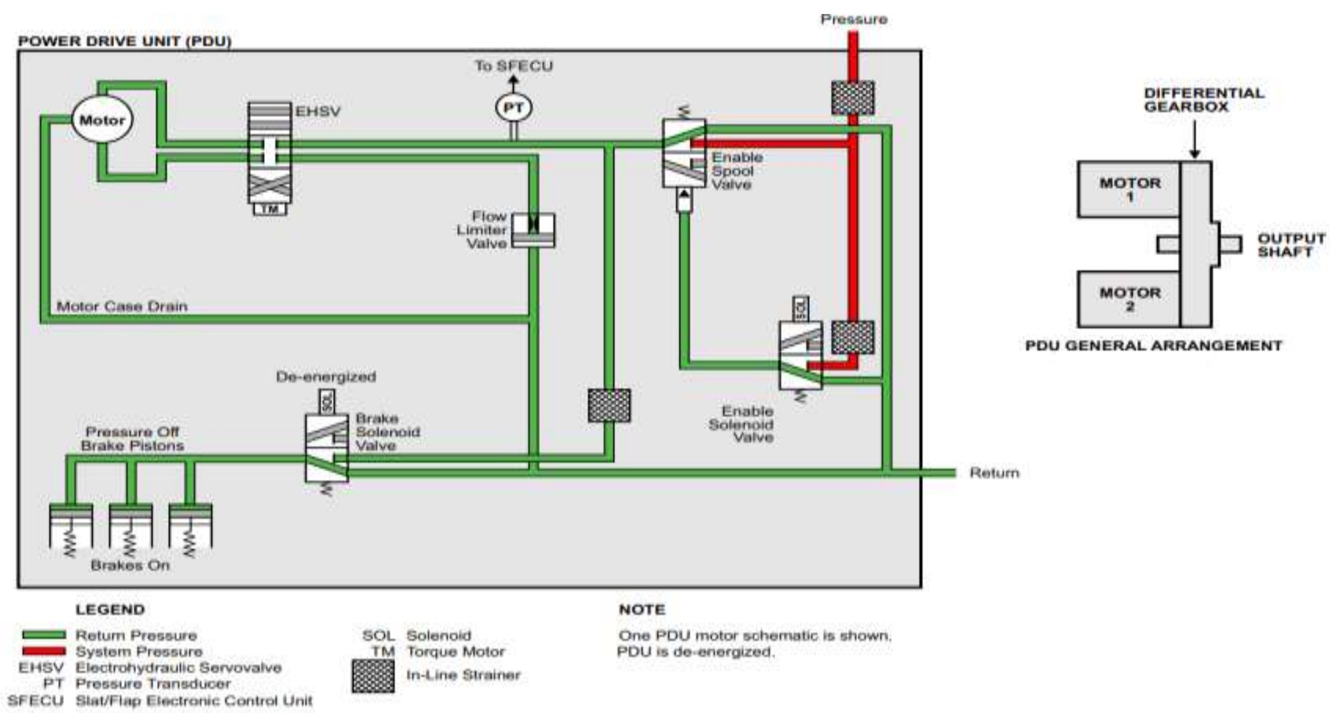

Figure 2.1: Power Drive Unit Schematic (BD-500-1A10 Technical Training Manual 2005).

2.2 Jet Pipe Electrohydraulic Servo Valves.

Jet pipe electrohydraulic servo valves operate by utilizing a high-velocity jet of hydraulic fluid to control the position of a valve spool. This mechanism provides significant advantages and disadvantages of jet pipe electrohydraulic servo valves (Davis et al., 2019).

2.2.1 Operational Mechanism.

The core principle behind JPEHSVs involves directing a fluid jet through a pipe, creating a differential pressure that influences the movement of the valve components. Research by Zhao et al. (2021) outlines how this mechanism allows for rapid changes in flow direction and rate, making JPEHSVs particularly effective in dynamic applications. In this type of servo valve, pilot pressure is applied to a jet pipe which, with a 50% control signal, directs an equal flow into two pilot lines. A change of control signal diverts the jet flow giving unequal flows and hence unequal pressures at the ends of the main spool. The main spool is linked mechanically to the jet pipe, causing it to move to counteract the applied electrical signal. Spool movement stops when the jet pipe is again centrally located over the two pilot pipes. This occurs when the main spool valve movement exactly balances the electrical control signal.

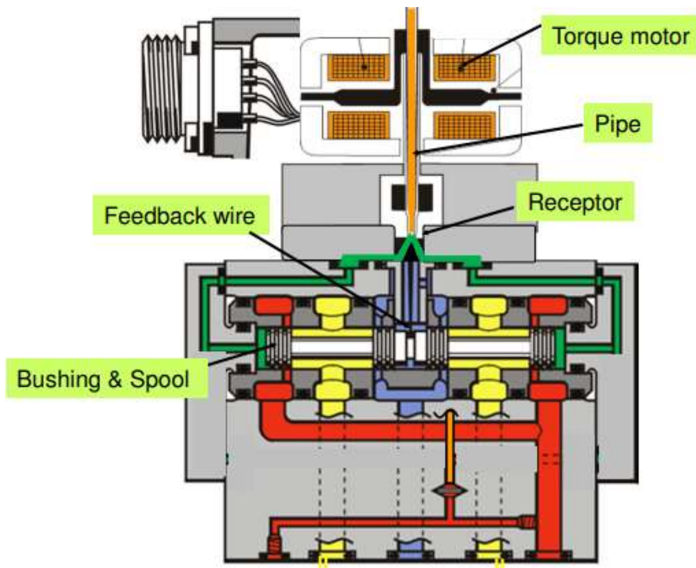

Figure 2.2: Jet pipe Electrohydraulic servo valve (Moog 1957).

2.2.2 Design Features.

JPEHSVs are characterized by their compact design and lightweight structure, which enhance their application in mobile and aerospace systems. Lee and Kim (2020) discuss the use of advanced materials and manufacturing techniques that optimize the performance and durability of these valves.

2.3 Two-Stage Nozzle Flapper Servo Valve (TSNF EHSV).

Two-stage nozzle flapper electrohydraulic servo valves (TSNF EHSV) are integral components in precision hydraulic systems, widely used in aerospace, industrial automation, and robotics. This survey discusses their design, operational principles, advantages, and applications, drawing on recent research.

Introduction to Two-Stage Nozzle Flapper Electrohydraulic Servo Valves

The two-stage nozzle flapper servo valve consists of a flapper mechanism that modulates flow through a nozzle. This design enhances control over hydraulic actuation by providing high gain and stability. As noted by Huang and Zhang (2021), the two-stage configuration allows for improved response characteristics and greater control precision compared to single-stage designs.

2.3.1 Operational Mechanism of (TSNF EHSV).

The operation of TSNF EHSV is based on a two-stage process:

First Stage: The flapper moves in response to an input electrical signal, adjusting the flow of hydraulic fluid through the nozzle.

Second Stage: The fluid flow generated by the first stage actuates a larger hydraulic piston, providing the necessary force to drive a load (Cai et al., 2020). This mechanism offers a significant amplification of the input signal, allowing for precise control over larger actuators (Lee et al., 2019).

2.3.2 Design Features

The design of TSNF EHSVs typically incorporates features such as:

High Precision: The nozzle flapper arrangement provides a linear response to input signals, enhancing control accuracy (Singh & Gupta, 2022).

Compact Size: These valves are designed to minimize size and weight, making them suitable for applications where space is limited, such as in aircraft (Davis & Brown, 2023).

2.4 Research Gap

Dasgupta et al (2011) introduced a modeling and simulation study that dealt with a comprehensive model of a closed-loop servo valve-controlled hydro motor drive system that has been made using (Bond graph simulation technique). The dynamic performance of the complete system has been studied to the variation of the parameters of the (PI) controller that drives the servo valve, they have also studied the effects of the variation of torque motor parameters on the servo valve performance.

Hossam et al (2011) introduced an experimental and theoretical study of the electrohydraulic servo system of speed control of hydraulic motors. The performance of the model-based control system depends strongly on the accuracy of the process model used. The least squares support vector machines method (LSSVM) is a powerful method for modeling nonlinear system results that show good performance over a wide range of operating conditions and load disturbances.

The present study investigated the performance of the servo valve in the aircraft wing flap actuation mechanism.

3.0 Methodology

3.1 Mathematical Modeling.

To be able to conduct modeling of the servo valve for aircraft wing flap actuation, all major components of the valve were listed and arranged in the form of a block diagram as shown in Figure 3.1.

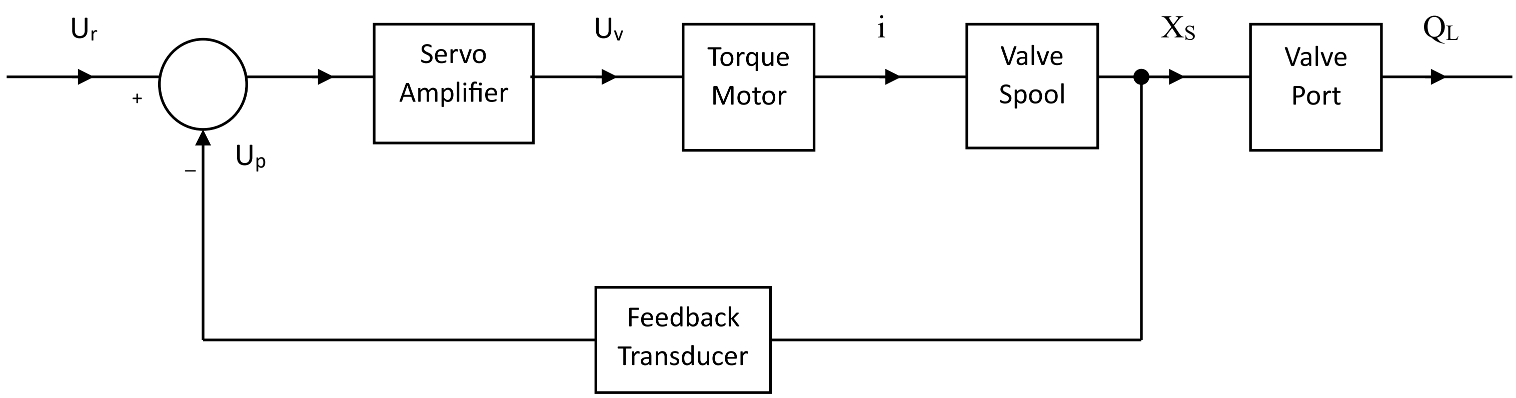

Figure 3.1: A block diagram of EHSV for Aircraft Wing Flap Actuation Mechanism.

Modeling of the EHSV was conducted after studying the operation of the aircraft flap actuation mechanism and its block diagram. By using the appropriate fundamental principles of fluid dynamics, mechanics, electrics, and control theory. mathematical equations describing the operation of each component, and their operational gains were developed.

3.1.1 Mathematical Modeling of an EHSV for Aircraft Wing Flap Actuation Mechanism.

The EHSV system considered in this design study consists of the following elements.

i. Servo Amplifier

ii. Torque Motor

iii. Valve spool.

iv. Valve port

v. Feedback transducer

3.1.2 Servo Amplifier Modeling.

The mathematical equation describing the relationship between the input voltage signal U and output voltage signal (control voltage U_v) of the servo amplifier is given below.

$$u_v(t) = K_s \cdot u(t) \quad \ldots\ldots\ldots\ldots\ldots\ldots\ldots\ldots\ldots\ldots(3.1)$$

To obtain the corresponding transfer function, use was made of laplace transform technique and equation 3.1 was express as:

$$U_v(s) = K_s \cdot U(s) \ldots\ldots\ldots\ldots\ldots\ldots\ldots\ldots\ldots\ldots(3.2)$$

Transfer function of the servo amplifier $G_v(S)$.

$$G_v(S) = \frac{Laplce\ transform\ of\ Output}{Laplace\ transform\ of\ Input}$$

$$G_v(S) = \frac{Uv(s)}{U(s)} = K_s = K_a \ldots\ldots\ldots\ldots\ldots\ldots\ldots\ldots\ldots\ldots\ldots\ldots\ldots\ldots(3.3)$$

Where K_a is the amplification factor of the servo amplifier, which is a gain term. $U_v(t)$ is the control voltage , U(t) is the input voltage to the servo mplifier.

The resulting block diagram of a servo amplifier is shown in Figure 3.3 below.

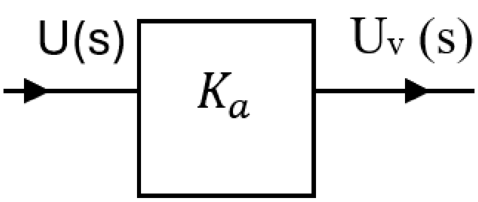

Figure 3.2: Servo Amplifier block diagram.

3.1.3 Torque Motor Modelling.

Considering the electrical characteristics of the servo valve torque motor, the mathematical equation describing the relationship between the control voltage signal $U_v(t)$ and the control current i(t) signal of the torque motor is given below.

$$L_c \frac{di}{dt} + R_c \cdot i(t) = K_a \cdot U_v(t) \ldots\ldots\ldots\ldots\ldots\ldots\ldots\ldots\ldots\ldots(3.4)$$

To obtain the corresponding transfer function, use was made of laplace transform technique and equation 3.4 was express in laplace transform as:

$$L_c s\, I(s) + R_c \cdot I(s) = K_a \cdot U_v(s) \quad \ldots\ldots\ldots\ldots\ldots\ldots\ldots\ldots\ldots\ldots(3.5)$$

Transfer function of the servo amplifier $G_v(S)$.

$$G_t(S) = \frac{Laplce\ transform\ of\ Output}{Laplace\ transform\ of\ Input}$$

$G_t(S) = \frac{\text{I(s)}}{\text{Uv(s)}} = \frac{1}{sL_C+R_C}$ …………………………………………… (3.6)

where L_c is the inductance of the torque motor coil, and R_c is the combined resistance of the torque motor coil and the current sense resistor, K_a the amplification of the servo amplifier, (K_a . U_v(s)) and i are the control voltage and current.

The resulting block diagram of a torque motor is shown in Figure 3.4 below.

$$U_v(s) \longrightarrow \boxed{\frac{1}{sL_c + R_c}} \longrightarrow I(S)$$

Figure 3.3: Torque block diagram.

3.1.4 Valve Spool Flow Modeling.

The valve spool of the servo valve is designed to give a displacement $X_s(t)$ that is directly proportional to the control current i(t). The mathematical equation describing the relationship between the control current i(t) and the valve spool displacement $X_s(t)$ is given below.

$$X_s(t) = K_t \, . \, i(t) \qquad \text{. ……………………… (3.7)}$$

where, X_s(t) is the valve spool displacement, K_t is the proportionality coefficient between the control current and valve spool displacement, i (t) is the control current.

The lateral force on the valve spool is expressed as:

$$F = M\frac{d^2X_s(t)}{dt^2} + \mu\frac{dX_s(t)}{dt} \qquad \text{………….…………… (3.8)}$$

Where M is the mass of the valve spool (Kg), μ is the spool viscous friction coefficient (kg/s).

Considering the compressibility of mineral oil hydraulic fluid in the system, the mathematical equation representing the relationship between the control current i(t) and the valve spool displacement X_s(t) is expressed as:

$$\frac{VM}{K_BA^2}\frac{d^2X_s(t)}{dt^2} + \frac{V\mu}{K_BA^2}\frac{dX_s(t)}{dt} + X_s(t) = K_t \, . \, i(t) \qquad \text{……………..…… (3.9)}$$

$$\frac{d^2X_s(t)}{dt^2} + \frac{\mu}{M}\frac{dX_s(t)}{dt} + \frac{K_BA^2}{VM}X_s(t) \quad = \frac{K_BA^2}{VM} . K_t \, . \, i(t) \text{ ……………… (3.10)}$$

To obtain the corresponding transfer function, use was made of laplace transform technique and equation 3.10 was express in laplace transform as:

Expressing in Laplace transforms.

$$S^2X_s(s) + \frac{\mu}{M}\, S\, X_s(s) + \frac{K_BA^2}{VM}X_s(s)_s = \frac{K_BA^2}{VM} . K_t . I(s) \text{……. (3.11)}$$

$$X_s(s)\left(S^2 + \frac{\mu}{M}\,S + \frac{K_B A^2}{VM}\right) = \frac{K_B A^2}{VM}.K_t.I(s) \ldots\ldots\ldots\ldots\ldots\ldots..(3.12)$$

Expressing equation 3.12 in form of Transfer function G_{sp}(s).

$$G_{sp}(\mathrm{s}) = \frac{Laplce\ transform\ of\ Output}{Laplace\ transform\ of\ Input}$$

$$\frac{X_s(S)}{II(S)} = \frac{\frac{K_B A^2}{VM}.K_t}{\left(S^2+\frac{\mu}{M}S+\frac{K_B A^2}{VM}\right)} \quad \ldots\ldots\ldots\ \ldots\ldots\ldots\ldots\ldots\ldots\ldots\ (3.13)$$

Where V is the volume of the hydraulic fluid trapped between the spool ends (m^3), A is the spool cross section area (m^2).

The resulting block diagram of a valve spool is shown in Figure 3.5 below.

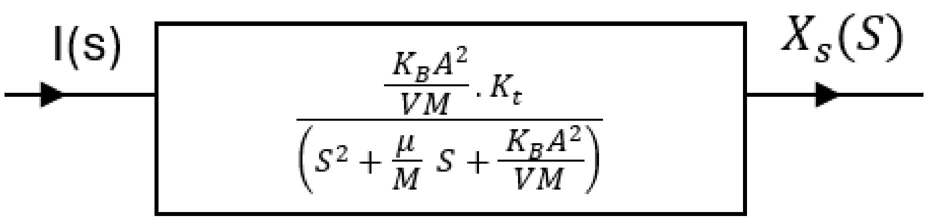

Figure 3.4: Valve spool block diagram.

3.1.6 Valve Port Modelling.

Due to the spool displacement as shown in Figure 3.6 below, the fluid is allowed to flow from pressure source (P_s) to chamber B and from chamber A to reservoir T. The rates of these flows can be calculated using equations given below.

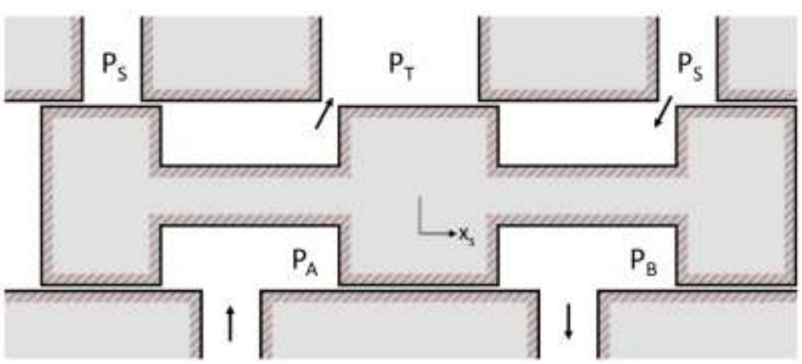

Figure 3.5: Valve spool displacement by lateral force.

$$Q_{PB} = C_{D,s} w X_s \sqrt{\frac{2}{\rho}(P_s - P_B)} \qquad \ldots\ldots\ldots\ldots\ldots...\ (3.14)$$

$$Q_{AT} = C_{D,s} w X_s \sqrt{\frac{2}{\rho}(P_A - P_T)} \quad \text{.....................} (3.15)$$

When the valve is open, Q_{PB} equals to Q_{AT}. Assuming $P_T = 0$.

$$C_{D,s} w X_s \sqrt{\frac{2}{\rho}(P_s - P_B)} = C_{D,s} w X_s \sqrt{\frac{2}{\rho} P_A}$$

$$P_s = P_B + P_A \quad \text{..............................} (3.16)$$

The pressure difference between the load ports is defined as the load pressure.

$$P_L = P_B - P_A \quad \text{..............................} (3.17)$$

Solving equations 14 and 15 together for P_A.

$$P_A = \frac{P_s - P_L}{2} \quad \text{..............................} (3.18)$$

Substituting equation 16 into equation 12.

$$Q_L = C_{D,s} w X_s \sqrt{\frac{P_s - P_L}{\rho}} \quad \text{..............................} (3.19)$$

Hence, the flow rate Q_L (t) flowing through a metering chamber of the main spool can be calculated as:

$$Q_L(t) = C_{D,s} w X_s(t) \sqrt{\frac{P_s - P_L}{\rho}}$$

Expressing equation 3.19 in Laplace transform.

$$Q_L(s) = C_{D,s} w X_s(s) \sqrt{\frac{P_s - P_L}{\rho}} \text{..............................} (3.20)$$

Expressing equation 3.20 in form of Transfer function G_{vp}(s).

$$G_{vp}(s) = \frac{Laplce\ transform\ of\ Output}{Laplace\ transform\ of\ Input}$$

$$G_{vp}(s) = \frac{Q_L(s)}{X_L(s)} = C_d w \sqrt{\frac{P_s - P_L}{\rho}} = K_3 \quad \text{..............................} (3.21)$$

where $C_{D,s}$ is the discharge coefficient in the metering chamber,

w is the slot width,

ρ is the oil density, and

$P_{s,} - P_{L,}$ is the pressure drop through the metering section.

$K_3 = valve\ port\ gain$

3.1.6 Feedback Transducer Modelling.

The sensed spool position $x(t)$ is converted into feedback electric signal $u_p(t)$ by the feedback transducer. The mathematical equation describing the relationship between the sensed spool position $x(t)$ and the feedback electric signal $U_p(t)$ is given by the equation 3.22.

$u_p(t) = K_v . x(t)$ …..………………………(3.22)

Where K_v is the coefficient of proportionality.

To obtain the corresponding transfer function, use was made of the Laplace transform technique, and equation 3.23 was expressed as:

$U_p(s) = K_v . X(s)$ ………………………………..…(3.23)

The transfer function of the feedback transducer $H(s)$.

$H(s) = \frac{Laplce\ transform\ of\ Output}{Laplace\ transform\ of\ Input}$

$H(s) = \frac{Up(s)}{X(s)} = K_v$ ……………………………………………(3.24)

Where K_v is the Feedback transducer gain (V/m)., $U_p(t)$ is the feedback electrical signal and $X_s(t)$ is the sensed spool displacement.

The resulting block diagram of a feedback transducer is shown in Figure 3.8 below.

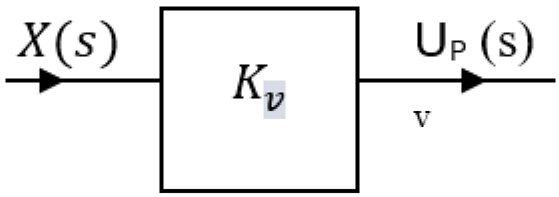

Figure 3.6: Feedback transducer block diagram.

3.2 Simulation Study.

MATLAB (Matrix Laboratory) is a high-level programming language and interactive environment primarily used for numerical computing, data analysis, algorithm development, and visualization. MATLAB is a versatile tool used across various fields for computation, analysis, and visualization. MATLAB also offers tools like Simulink for modeling and simulating dynamic systems with a graphical interface, which can simplify some aspects of simulation studies. The simulation studies carried out in this study aimed to observe the time response of each servo valve component to its step inputs.

4.0 Results and Discussion

This study focused on presenting the general servo valve performance for the designated design parameters as well as the simulation findings of the experimental investigations carried out with the use of MATLAB computer software for each servo valve component. To clarify the servo valve's behavior and response to the step inputs, a discussion of the findings was provided.

4.1 Simulation and Simulation Results of Servo Amplifier Model.

The weak input voltage U of the electrohydraulic servo valve is amplified by the servo amplifier to obtain a suitable control voltage U_v.

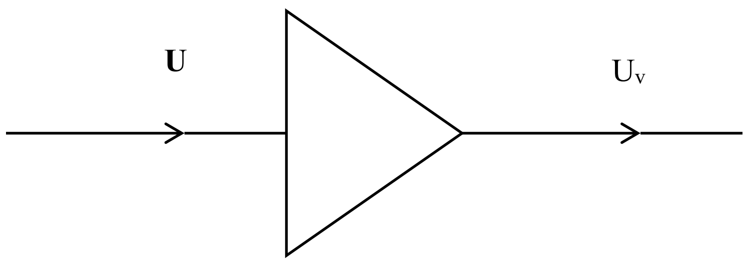

Figure 4.1: Servo amplifier

The amplification factor of the servo amplifier is termed the servo amplifier gain. K_a Is the design parameter considered in this study. According to the aircraft technical manual, the control voltage U_v ranges from 0 to 10V. The step input voltage U has been considered in the range of 0.2 to 1.0 volts and the servo amplifier gain is 5, thus. $K_a = 5$. Consider Table 4.1.

Table 4.1: Table of Step input voltage U and control voltage U_v.

STEP INPUT VOLTAGE, U (volts).	**CONTROL VOLTAGE, U_v** $U_v = K_a . U$ **(volts)**
0.2	1
0.4	2
0.6	3
0.8	4
1.0	5

Step input voltage simulations of a servo amplifier simulated with the aid of MATLAB computer software produced the step response graph shown in Figure 4.1 below.

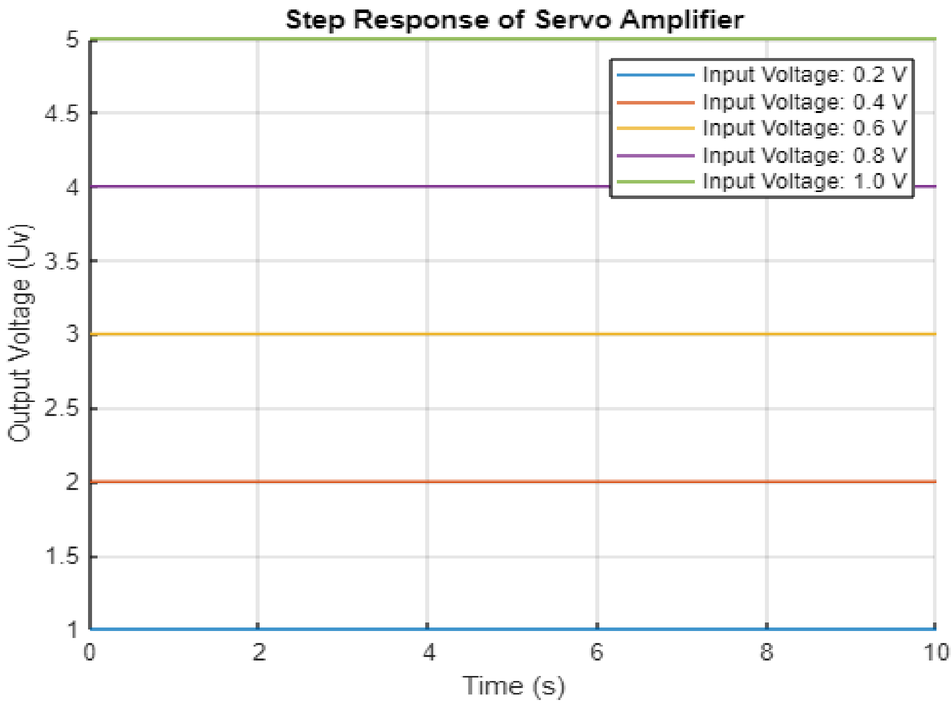

Figure 4.2: Step response of servo amplifier with various input voltage.

4.1.1 Servo Amplifier Model Simulation Results.

The results obtained after simulating the step inputs voltage of 0.2,0.4,0.6,0.8 and 1V in MATLAB software for servo amplifier gain $K_a = 5$, is an output (Control) voltage 1,2,3,4, and 5V. The results obtained are suitable for application in aircraft wing flap actuation mechanisms since they are within acceptable range,

4.2 Simulation and Simulation Results of Torque Motor Model.

When the control voltage from the servo amplifier is fed to the torque motor, electric current (Control current). Flows through the torque motor coils. The torque motor coil resistance R_c and coil inductance L_c Are the design parameters of the torque motor determining the output (control) current? These are the parameters that were considered in this research study. The torque motor coils conduct electric current (control current) when the torque motor receives the control voltage from the servo amplifier. To determine the output (control) current, the torque motor's design parameters are the coil resistance R_C and coil inductance L_c. These are the criteria taken into account in this investigation.

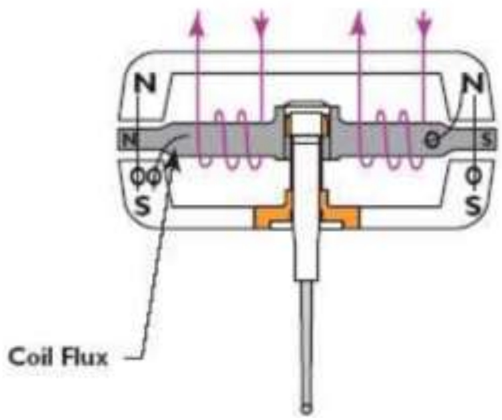

Figure 4.3: Torque Motor.

According to the manufacturer's datasheet, the value of torque motor coil inductance ranges from 10 to 100mH, torque motor coil resistance ranges from 10 to 100,Ω and control current 0 to 20mA. Table 4.2 shows the simulation results of the step input control voltage to the torque motor and the control current (output).

Table 4.2: Table of step control voltage and control current for the torque motor.

STEP CONTROL VOLTAGE, U_v (volts)	**CONTROL CURNT $\frac{Uv}{0.06S+70}$ (mA)**
1	15
2	30
3	42
4	57
5	70

Step control voltage simulations of a torque motor simulated with the aid of MATLAB computer software produced the step response graph shown in Figure 4.4.

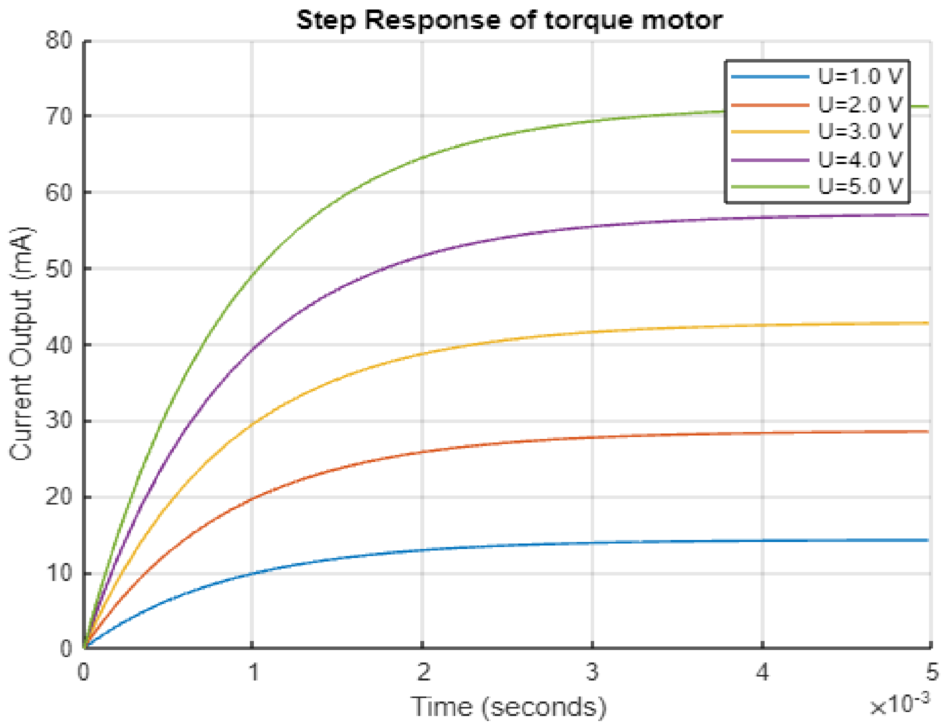

Figure 4.4: Step response of torque motor with various control voltage.

4.2.1 Torque Motor Simulation Results.

The results obtained after simulating the step control voltage of 1,2,3,4 and 5V in MATLAB computer software for torque motor with coil resistance and coil inductance of 70Ω and 0.06H respectively, was an output (Control) current of 15,30,42,57 and 70mA respectively. The result corresponding to the assigned design parameters was found suitable for application in aircraft wing flap actuation mechanism since it falls within the recommended range.

4.3 Simulation and Simulation Results of Valve Spool Model.

When the current flows through the torque motor coil, electromagnetic forces are generated and rotate the armature and the flapper assembly creating pressure difference at the spool ends. The pressure difference results in the spool displacement. $X_s(t)$ Which is proportional to the control current. The valve spool design parameters include a mass of the spool M, volume of the fluid trapped at the end of the spool V, control current coefficient. K_t, spool and spool cross-section area A.

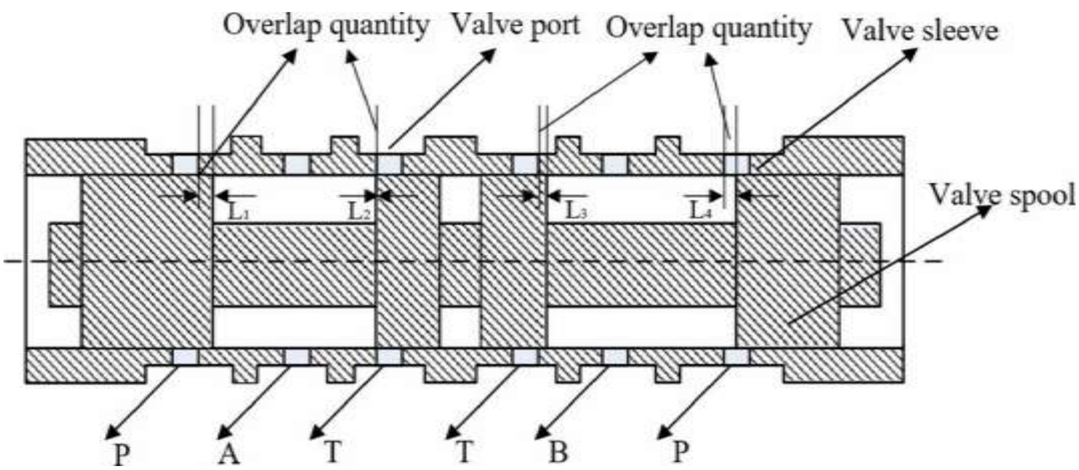

Figure 4.5: Valve Spool.

Table 4.3: Table of step control current and spool displacement for the valve spool.

CONTROL CURRENT I (A)	**SPOOL DISPLACEMENT X_s (m)** $X_s = \frac{\frac{K_B A^2}{VM} . K_t \, . \; i}{\left(S^2 + \frac{\mu}{M} S + \frac{K_B A^2}{VM}\right)}$
0.015	0.0006
0.030	0.00116
0.042	0.0016
0.057	0.0022
0.070	0.0027

Step control current simulations of the valve spool simulated with the aid of MATLAB computer software produced the step response graph shown in Figure 4.6.

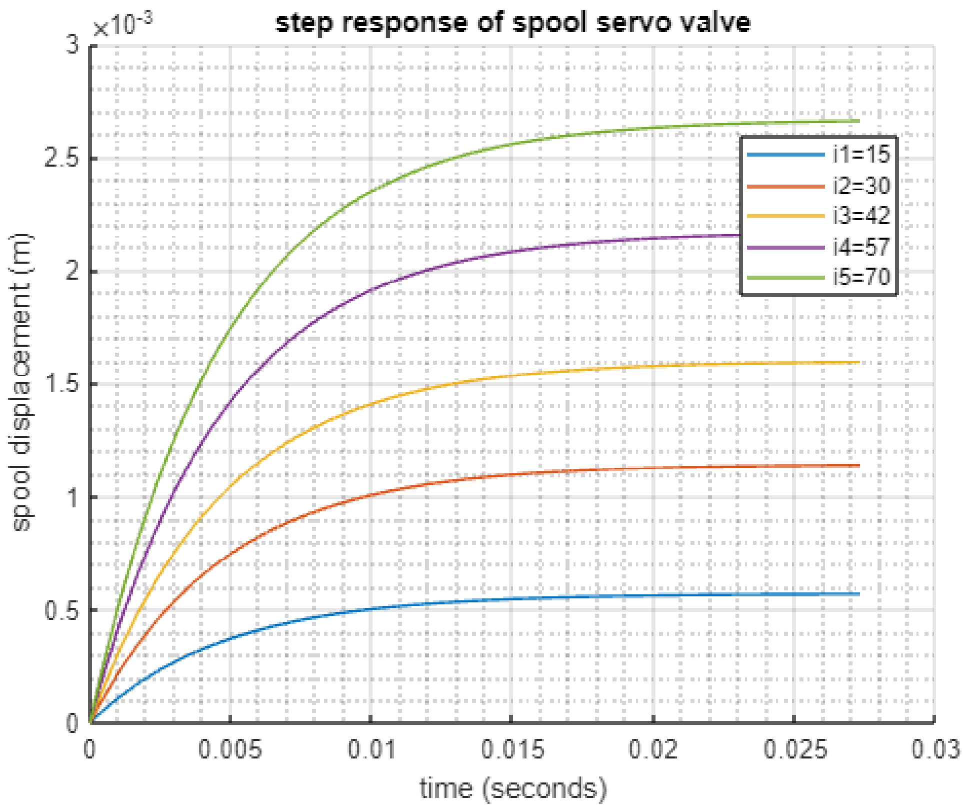

Figure 4.6: Step response of valve spool with various control voltage.

4.3.1 Valve Spool Simulation Results.

The results obtained after simulating the step control current of 0.015,0.03,0.042,0.057 and 0.07A in MATLAB computer software for a valve spool with the following design parameters *V= 49.2* mm^3, *A*= $16.76\ x\ 10^{-6}m^2$, $K_t = 38.1\ x\ 10^{-3}m/A$ *and M= 0.0031Kg,* were spool displacement values of 0.6,1.16, 1.6,2.2, and 2.7mm. The results corresponding to the assigned design parameters were found suitable for application in aircraft wing flap actuation mechanisms since they resulted in valve displacement values that are within the recommended range.

4.4 Simulation and Simulation Results of Valve Port Model.

When the spool valve is displaced, the valve port opens allowing the fluid to flow from the tank to the hydraulic motor. The design parameters of the valve port include the discharge coefficient. $\boldsymbol{C_D}$ and the valve port width w. The values of the discharge coefficient and valve port have been considered 0.77 and 0.0012m.

Table 4.4: Table of step spool displacement $\boldsymbol{X_s}$ and valve flow rate.

SPOOL DISPLACEMENT X_s (m)	$\boldsymbol{Q_L}$ $(\boldsymbol{m^3}/\mathbf{s})\boldsymbol{Q_L} = (0.77)(0.0012)X_s\sqrt{\frac{(4000\ x\mathbf{10^5})}{860}}$
0.0006	$3.78\ x\ 10^{-4}$
0.00116	$7.3x\ 10^{-4}$
0.00160	$1x\ 10^{-3}$
0.0022	$1.39x\ 10^{-3}$
0.0027	$1.7\ x\ 10^{-3}$

Step spool displacement simulations of the valve port simulated with the aid of MATLAB computer software produced the step response graph shown in Figure 4.7.

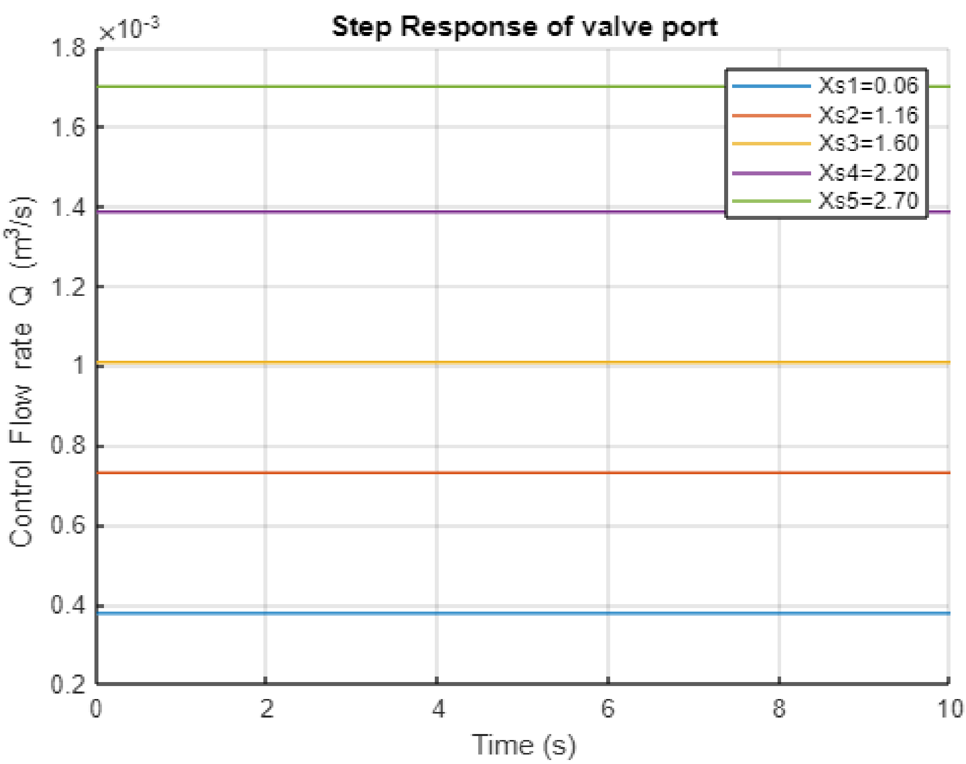

Figure 4.7: Step response of Valve port with various spool displacements.

4.5 Servo Valve Performance.

The simulation results exhibited how changes in input signals impact spool displacement and flow rate to the hydraulic motor for flap actuation, providing insights into the optimization of control strategies. The developed servo valve model is a second-order model that exhibited both transient and steady-state characteristics when simulated with various step inputs. Initially, both the spool displacement X_s and the control flow rate Q_L increased rapidly and overshot the steady state value, and eventually settled at an appropriate value, in response to a step input.

4.5.1 Step Response of Spool Displacement.

The time response of the spool displacement for a two-stage nozzle-flapper electrohydraulic servo valve for use in aircraft flap actuation mechanism showed a rapid increase in displacement due to the immediate effect of the step input. The spool displacement overshot beyond the steady state to 3.6mm, indicating a tendency of the servo valve to respond aggressively to changes. The spool then settled towards the spool equilibrium position 2.7mm. Damping characteristics were exhibited removing oscillations to attain a stable state. Consider Figure 4.8.

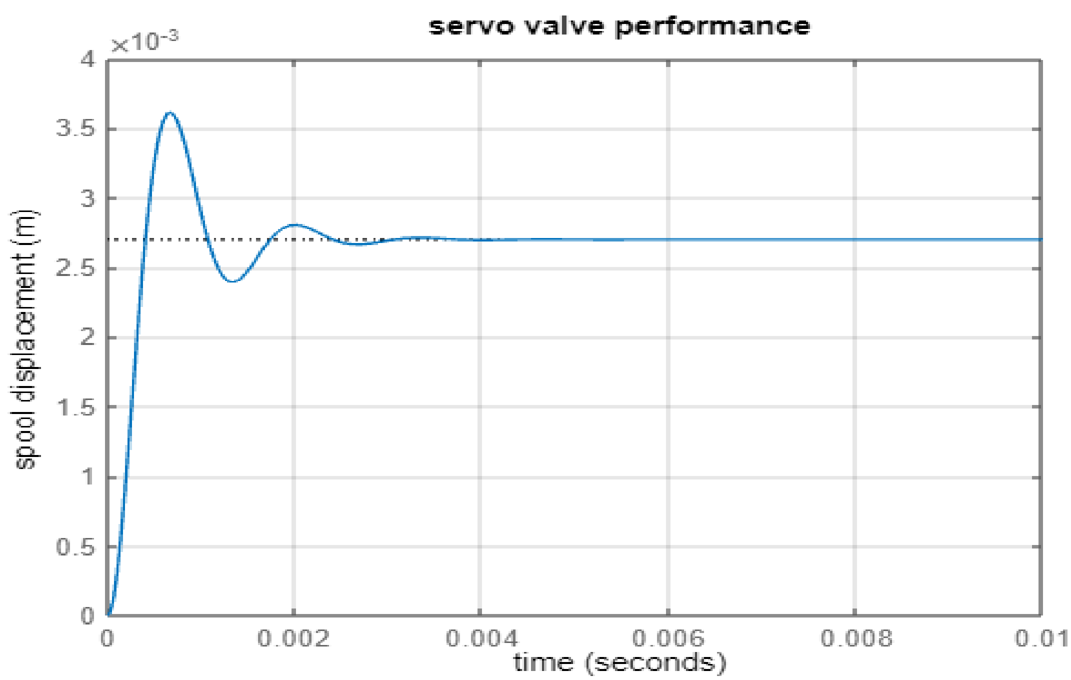

Figure 4.8: Step response of spool displacement X_s

The simulation results exhibit the following parameters for the spool displacement model of the tolerance band of plus or minus 0.1.

Table 4.5: table showing time parameters of the servo valve performance.

Details	Value
Delay time	0.0004s
Rise time	0.0003s
Maximum overshoot time	0.0008s
Settling time	0.002s

4.5.2 Step Response of Control Flow Rate Q_L.

The time response of the control flow Q_L A two-stage nozzle-flapper electrohydraulic servo valve for use in aircraft flap actuation mechanism showed a rapid increase in flow rate due to the immediate effect of the step input. The control flow rate overshot beyond the steady state to 2.35 $x\ 10^{-3}\ m^3/s$, indicating a tendency of the servo valve to respond aggressively to changes. The flow rate then settled towards the equilibrium flow of 1.75 $x\ 10^{-3}\ m^3/s$, Damping characteristics were exhibited removing oscillations to attain a stable state. Consider Figure 4.9.

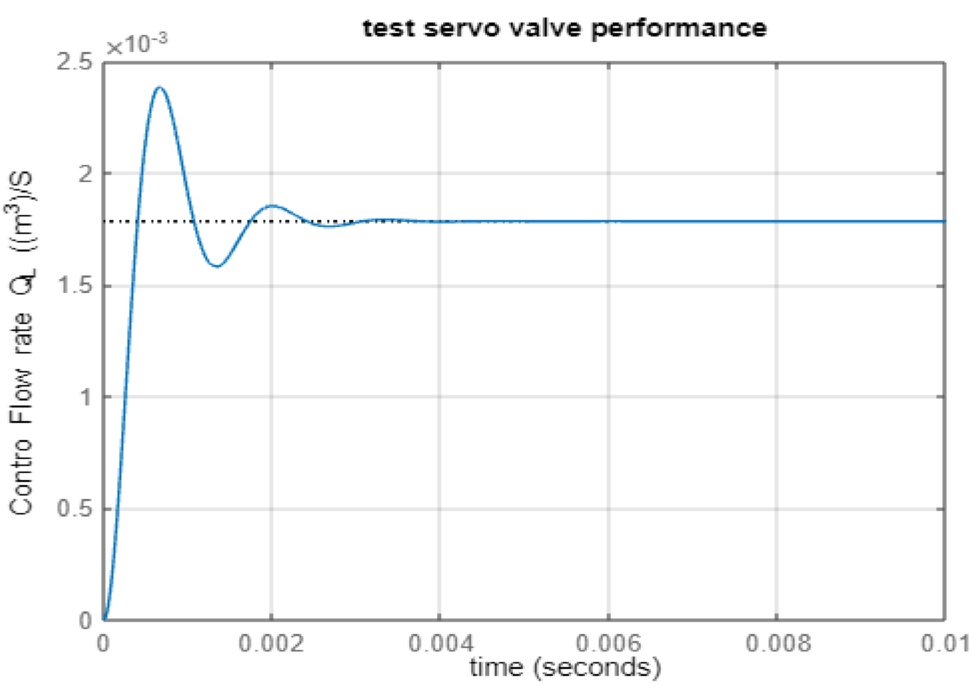

Figure 4.9: Step response of servo valve Control Flow rate $\boldsymbol{Q_L}$

The simulation results exhibit the following parameters for the control flow rate model of the tolerance band of plus or minus 0.1 m^3/s.

Table 4.6: table showing time parameters of the servo valve performance.

Details	**Value**
Delay time	0.0004s
Rise time	0.0005s
Maximum overshoot time	0.0009s
Settling time	0.002s

.

The electrohydraulic servo valve model simulation results elaborate the electrohydraulic actuation mechanism responsible for controlling the aircraft's wing flaps. Model simulation results mainly involved hydraulic dynamics which described fluid flow rate delivered to the hydraulic motor and valve dynamics describing the response characteristics of the servo valve spool displacement.

Conclusion

To design a servo valve model for an aircraft wing flap actuation mechanism, this study first determined the initial design parameters (such as coil resistance and inductance, spool mass, and area) required for the servo valve model. Next, the servo valve and its components (such as the torque motor, servo amplifier, valve spool, valve port, and feedback transducer) were mathematically modeled.

Optimized servo valve settings were achieved by adjusting original design factors such as spool mass and cross-section area. This study's optimization of several servo valve design parameters emphasizes how important precise control is to improve the efficiency and dependability of aircraft wing flap actuation mechanisms, which are essential for boosting safety during crucial flight phases like takeoff and landing.

By using the developed mathematical models of the servo valve and its components, MATLAB simulations conducted reveal the servo valve performance and its time responsiveness behavior. Time response study for each component has enabled us to determine the behavior of each component toward small changes in its input.

The time response simulation results of the designed servo valve model have been compared with the MOOG servo valve data. The time response graphs which are obtained by this simulation of the servo valve model for aircraft wing flap actuation mechanism are found to coincide with the experimental time response graphs of the Moog servo valve.

The results obtained indicate that optimized design parameters can lead to improved response times and accuracy in flap positioning, which directly influences overall aircraft performance.

REFERENCES

Cai, L., Zhang, Y., & Huang, X. (2020). Analysis of Two-Stage Nozzle Flapper Electrohydraulic Servo Valve Dynamics. Journal of Fluid Power Systems, 30(1), 15-28.

Davis, M., & Brown, A. (2023). Performance Characteristics of Two-Stage Nozzle Flapper Valves in Aerospace Applications. Aerospace Science and Technology, 105, 105891.

Huang, X., & Zhang, Y. (2021). Design Optimization of Two-Stage Electrohydraulic Servo Valves for Precision Control. Journal of Mechanical Engineering, 67(4), 213-225.

Kumar, R., & Patel, S. (2023). High Gain and Stability in Two-Stage Nozzle Flapper Electrohydraulic Valves. Control Engineering Practice, 137, 105675.

Lee, J., Park, H., & Kim, S. (2019). The Role of Flapper Mechanisms in Electrohydraulic Control Systems. International Journal of Hydraulics, 44(2), 99-112.

Lopez, R., & Martinez, A. (2021). Robotic Applications of Two-Stage Nozzle Flapper Valves: Performance Insights. Robotics and Automation Magazine, 28(3), 78-88.

Singh, A., & Gupta, P. (2022). Precision and Linearity in Electrohydraulic Servo Valve Design. Journal of Applied Mechanics, 89(3), 342-356.

Tran, D., Nguyen, H., & Pham, T. (2023). Smart Control Systems in Electrohydraulic Applications: Enhancements and Innovations. Journal of Fluid Power Technology, 56(2), 134-145.

Wang, L., Chen, Y., & Zhao, M. (2022). Advancements in Two-Stage Nozzle Flapper Valve Technology for Automated Systems. International Journal of Automation and Control, 19(1), 23-39.

Williams, K., & Johnson, M. (2022). Aerospace Applications of Two-Stage Electrohydraulic Servo Valves. Journal of Aerospace Engineering, 40(1), 30-45.

Zhao, L., Wu, J., & Li, F. (2023). Recent Trends in Hydraulic Servo Valve Technology for Manufacturing. Journal of Manufacturing Systems, 63, 85-97.

G. Qiao, G. Liu, Z. Shi, et al., “A review of electromechanical actuators for more/all electric aircraft systems,” Journal of Mechanical Engineering Science, Vol. 232, Part C, 2018.

Garg et al. Application of fiber optics in aircraft control system & its development. 2014 International Conference on Electronics and Communication Systems (ICECS).

J. Li, Z. Yu, Y. Huang, and Z. Li, “A review of electromechanical actuation system for more electric aircraft,” IEEE/CSAA International Conference on Aircraft Utility Systems (AUS), Beijing, China, Oct. 2016. doi: 10.1109/AUS.2016.7748100.

J.-C. Maré and M. Budinger, “Comparative analysis of energy losses in servo-hydraulic, electro-hydrostatic and electro-mechanical actuators,” 11th Scandinavian International Conference on Fluid Power, 2009.

J.-C. Maré, "Review and analysis of the reasons delaying the entry into service of power-by-wire actuators for high-power safety-critical applications," Actuators, vol. 10, no. 9, 2021, issn: 2076-0825. doi: 10.3390/ act10090233.

J.-C. Maré, Aerospace Actuators 2. St George's Road, London: ISTE, 2017.

J.-C. Maré, Aerospace Actuators 3. St George's Road, London: ISTE, 2018.

Joshi, A. and Jayan, P.G., Modelling and Simulation of Aircraft Hydraulic System, AIAA Paper No. AIAA-2002-4611, Proc. of Modelling and Simulation Technologies Conference, Monterey, CA, USA, 6-8 August 2002.

Randall T. Anderson Mathematical Modeling of a Two Spool Flow Control Servovalve Using a Pressure Control Pilot, ASME journal, volume 124, September 2004.

Lee et al. Achieving High-Performance Electrified Actuation System with Integrated Motor Drive and Wide Bandgap Power Electronics.

M. Bildstein, "A built-in jam release device for electromechanical actuators in flight control," Proceedings of the 6th International Conference on Recent Advances in Aerospace Actuation Systems and Components, Toulouse, France, pp. 105–108, 2–3 April, 2014.

Meredith PT. Viscious phenomena affecting High-lift systerms and suggestions for future CFD development. AGARD conference proceedings 515, 1993.

Panagiotis, detailed model of an electro hydraulic servo system International journal of fluid power, volume 5, number 2, September 2004, pp 121-138.

Qiao et al. A review of electromechanical actuators for More/All Electric aircraft systems.

Qiao et al. Friction Torque Modelling and Efficiency Analysis of the Preloaded Inverted Planetary Roller Screw Mechanism.

Randall T. Anderson Mathematical Modeling of a Two Spool Flow Control Servovalve Using a Pressure Control Pilot, ASME journal, volume 124, September 2004.

Rudolph PKC. Mechanical design of high lift systems for high aspect ratio swept wings. Washington, D.C.: NASA；1998. Report No.: NASA/CR-1998-196709.

Rudolph, P.K.C.: 'High-Lift Systems on Commercial Subsonic Airliners'. NASA Contractor Report 4746, September 1996

S. Frischemeier, "Electrohydrostatic actuators for aircraft primary flight control-types, modelling and evaluation," Proceedings of the Fifth Scandinavian . . ., pp. 1–16, 1997. doi: 10.15480/882.236.

Smith AMO. High-lift aerodynamics. J Aircraft 1975;12 (6):501–30.

Y. Hussain, S. Burrow, L. Henson, and P. Keogh, "A review of techniques to mitigate jamming in electromechanical actuators for safety critical applications," International Journal of Prognostics and Health Management, vol. 9, no. 12, 2018, issn: 2153-2648, 2018 012.

Recksiek, M.:(2009), 'Advances high lift system architecture with distributed electric flap actuation'. – (AST), Hamburg, Germany

Hardwick, G., Hanna, S., Panella, I.: 'Functional modelling of high lift systems'. NAFEMS World Congress, 2017s